ELSEVIER

Chemical Engineering Journal 128 (2007) 95–104

Chemical Engineering Journal

www.elsevier.com/locate/cej

Studies on bubble dynamics with mass transfer

T. Madhavi, A.K. Golder, A.N. Samanta, S. Ray *

Department of Chemical Engineering, IIT Kharagpur, Kharagpur 721302, India

Received 21 March 2006; received in revised form 10 October 2006; accepted 18 October 2006

Abstract

The dynamics and mass transfer of a single reactive bubble of carbon dioxide rising in a strong alkaline solution of sodium hydroxide has been investigated experimentally and numerically. A simple dynamic model of the bubble based on pressure balance, force balance and mass transfer considerations has been developed. The model assumes sphericity of bubble and considers added mass of liquid, drag and surface tension effects on bubble pressure. The effect of the accumulated contaminants on the mass transfer and drag coefficients are included in the model using an adaptation from literature. Photographic technique has been successfully used to follow the radius, and rise of the individual CO_2 bubbles of radius ranging from 0.45 to 0.65 mm rising in 4%, 6% and 10% (w/v) NaOH solutions. The rise velocity, drag coefficient, mass transfer coefficient and other parameters were calculated from the videograph.

Limited deviation between model and experiments expressed as absolute deviation in radius (mean: 6.89%, maximum: 12%), velocity (mean: 8%, maximum: 24%), and rise (mean: 7.3%, maximum: 15%) is observed. The enhancement factor for the mass transfer with reaction, the cap angle of the accumulated contaminants and drag coefficient were calculated from the model.

Keywords: Mass transfer; Bubble; Numerical analysis; Hydrodynamics; Absorption; Sodium hydroxide

1. Introduction

Understanding of bubble motion mechanism is essential for many gas–liquid and liquid–liquid operations. Though practical processes involve bubbles swarms, study of behavior of the single bubble gives insight into the overall. This makes the mass transfer to (or from) a single bubble an essential base for better understanding of liquid–liquid extraction or gas–liquid absorption processes with or without reactions. A vast number of publications in this field of study reflect the importance of the area. The present work concentrates on single bubble behavior, by itself a quite complex problem, particularly when the purpose is to cover a range of liquid phase properties and bubble size.

The motion of the bubbles and drops has aroused a lot of interest for many years and the earliest investigations were carried out by Rybczynski (1911) [1] on a liquid–liquid system. Mass and heat transfer around a fluid sphere were studied by Kinard et al. [2] and Ruckenstein [3]. Tsuge et al. [4] experimentally investigated the wall effect on the terminal velocity and the shape of single bubbles rising in highly viscous liquid. Griffith [5], Clift et al. [1], Sadhal and Johnson [6], Tzounakos et al. [7], Vizquez et al. [8], and Vasconcelos and coworkers [9,10] observed the effect of the contamination. It was also reported that a very small amount of contaminant affects the bubble behavior. Real bubbles in most cases pick up dirt/impurities very quickly and the behavior is different from uncontaminated bubbles. Takemura and Yabe [11] and Takemura and Matsumoto [12] investigated experimentally and numerically the gas dissolution process of a spherical rising gas bubble using a charged coupled device (CCD).

2. Experimental apparatus and procedures

The experimental setup for the study of the change in the bubble size and its hydrodynamics is shown in Fig. 1. It consists of a test section, a bubble generating system, a light source, a high-speed digital camera and a computer connected to the camera. The test section (1) was a glass walled 96 mm^2 column, 100 mm tall, mounted on a stand. A rubber cork was provided at the base of the column to grip the needle. The bubble generating system (3) consists of hypodermic syringe. The bubbles

* Corresponding author. Tel.: +91 3222 283944; fax: +91 3222 282250.
E-mail address: sray@che.iitkgp.ernet.in (S. Ray).

1385-8947/$ – see front matter © 2006 Elsevier B.V. All rights reserved.
doi:10.1016/j.cej.2006.10.019

Nomenclature

$a, \dot{a}, \ddot{a}$	bubble radius (mm) and its time derivative
a_s	area occupied by 1 mol of contaminant (m^2)
a_0	initial bubble radius (mm)
A	cross-sectional area of the column (m^2)
A_b, A_{cap}	area of the bubble and area occupied by the contaminant (m^2)
C_{A0}	solubility of CO_2 in water (kg/m^3)
C_{B0}	concentration of NaOH in bulk liquid (mol/m^3)
C_D	drag coefficient
C_∞	contaminant concentration in the bulk (mol/m^3)
D_B, D_A	diffusivity of NaOH, dissolved CO_2 in NaOH solution (m^2/s)
g	gravitational gas constant (m/s^2)
h	height of liquid above orifice (m)
H	Henry's constant (m^3 $(N/m^2)/(kg\ mol)$)
k	parameter in the contaminant growth equation ($m^{1/2}/s$)
k_{LA}, k_s	liquid phase mass transfer coefficient, mass transfer coefficient of the surfactant (m/s)
k_r	reaction rate constant ($m^3/(mol\ s)$)
M_w	molecular weight
n_b, n_s	number of moles inside the bubble, moles of the contamination accumulated in the stagnant cap
n_{b0}	initial number of moles inside bubble
p_b	pressure inside the bubble (N/m^2)
p_{b0}	initial bubble pressure (N/m^2)
p_0	atmospheric pressure (N/m^2)
R	ideal gas constant (m^3 $(N/m^2)/(K\ kg\ mol)$)
Re	Reynolds number
S	bubble rise (mm)
T	operating temperature (K)
t	time (s)
V, $\dot{V}$	bubble volume (m^3) and its time derivative
z	number of OH^- ions reacting with one molecule of CO_2

Greek letters

θ	stagnant cap angle (°)
ρ_b, ρ_l	density of gas and liquid (kg/m^3)
σ	surface tension force (N/m)

were injected manually into the column ensuring that a single bubble was introduced at a time. A light source (2) was used to provide the necessary illumination for the photography. The motion and dissolution of the bubbles were followed by a low-light high-speed digital camera (4) mounted on a well-balanced adjustable platform. The camera used was Basler A-301-b, 8 bit. It can film sequences up to 80 frames/s and the output video signal was acquired in the computer (5). The recorded sequence of bubble motion was analyzed by using image processing software (Adobe Photoshop 7.0). Calibration of the vision field is made by photographing a precision scale placed along the bubble displacement axis.

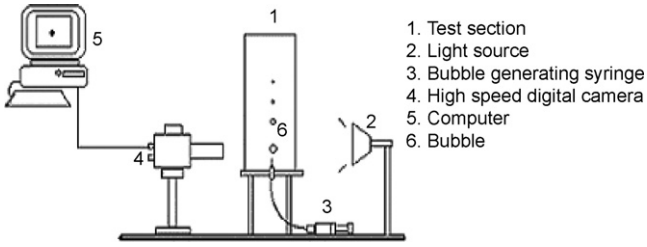

Fig. 1. Schematic illustration of the experimental setup.

This initial adjustment of the camera and the light source was done using air-water system to avoid the heat effects on the CO_2–NaOH system due to the excessive warming of the solution by the light source during the adjustments.

The test section is filled with NaOH solution of known concentration up to a height of 57 mm and CO_2 bubbles of radius varying from 0.3 to 0.65 mm were injected manually into NaOH solution. The dissolution of the CO_2 bubbles during their flight is due to their absorption associated with chemical reaction with NaOH solution. The rise and dissolution of the bubble were captured by the camera at 80 frames/s. The radius was measured in every frame and the velocity was calculated by measuring the change in position of the centre of the bubble from frame to frame.

The effect of initial bubble radius and the initial concentration of the NaOH solution are observed. To study the effect of the concentration of the NaOH on the absorption of CO_2 three different concentrations of 4%, 6%, and 10% (w/v) NaOH solutions were used. All experiments were carried out at local ambient temperature (25–30 °C) and under atmospheric pressure (762 ± 1 mm Hg). The physical properties of NaOH and CO_2 at these conditions are given in Table 1. Fig. 2 shows photographs of typical rising bubble taken with the high-speed camera, which show the dissolution of CO_2 bubbles in the NaOH

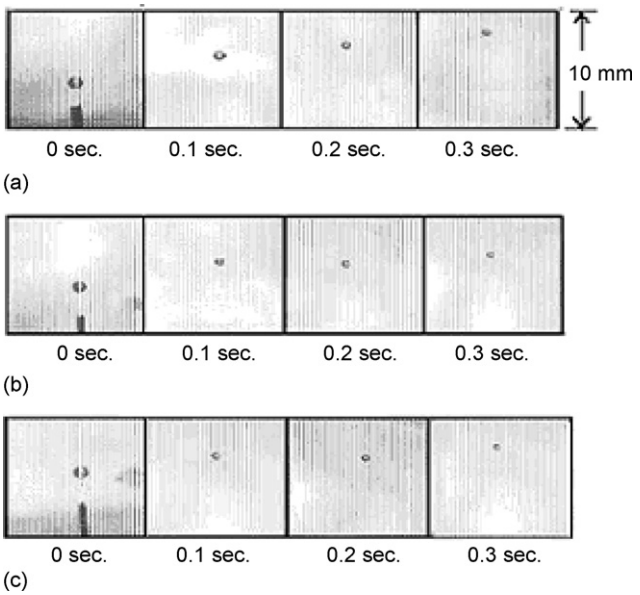

Fig. 2. Photographs of typical rising bubble in (a) 4%, (b) 6% and (c) 10% NaOH solutions.

Table 1
Physical properties of NaOH solution and CO_2

Property	Reference	4% NaOH	6% NaOH	10% NaOH
Density (kg/m^3)	Measured using Sp. Gr. bottle	1042	1066.7	1106.6
Viscosity (Pa s)	http://www.oxy.com/OXYCHEM/Products/caustic_soda/literature/caustic%5B1%5D.pdf	1.25×10^{-3}	1.35×10^{-3}	1.6×10^{-3}
Diffusivity of CO_2 (m^2/s)	Calculated by the method proposed by Gordon given in [22]	1.53×10^{-9}	1.425×10^{-9}	1.202×10^{-9}
Henry's constant of CO_2 in NaOH (N/m^2) m^3/kgmol	Calculated by the method proposed by van Krevelen and Hoftijzer given in [19]	3.5698×10^6	4.1845×10^6	5.7498×10^6

solution. These are clipped from the original photographs and the vertical position of bubbles should not be deduced from there. The non-sphericity of the bubbles with different initial radii was estimated by the quantity $(1 - R_{min}/R_{max})$, where R_{min} and R_{max} are the measured minimum and maximum radius for a particular bubble in a captured image. For the bubbles in general during experiments, the non-sphericity value was 0.03 maximum and this is regarded as small. Therefore, the bubbles are considered as spherical under the experimental conditions. It is also well known that the deformation of the bubble strongly depends on the Weber number and the bubble deformation is negligibly small when Weber number is smaller than 0.5 [11]. The Weber numbers were 0.342, 0.416 and 0.595 for 4% NaOH solution and hence the bubbles are considered spherical.

3. Mathematical formulations

A single bubble of CO_2 of radius 'a' is considered to rise in a pool of NaOH solution through a height 'h'. The bubble rises and reduces in size due to its reaction/mass transfer with NaOH solution. However, there is also tendency for the bubble to grow as it rises and its pressure falls. The net change in bubble size is therefore the result of two opposing tendencies. At $t = 0$, the observation starts and the bubble is considered to be at a height 's' from the reference plane. Following are the assumptions made during modeling the system mathematically:

(1) Heat effects during dissolution are not significant. So the process is assumed to be isothermal.
(2) Liquid phase resistance controls mass transfer.
(3) Bubble is small and therefore spherical.
(4) Concentration of dissolved CO_2 is in equilibrium with bubble pressure.
(5) Concentration of solute gas in the bulk liquid phase is assumed to be zero.
(6) Velocity of bubbles is not affected by oscillations in the range of the bubble radius considered [13].
(7) Effects of the confining wall on the bubble are neglected.
(8) The interfacial tension is assumed to be constant.
(9) The contaminant is considered to be accumulating on the interface.

3.1. Momentum transfer

The equations for bubble growth and bubble rise are developed by considering the pressure balance and force balance over the bubble [14,15].

3.1.1. Pressure balance on the bubble

The bubble grows when the pressure inside the bubble (p_b) exceeds the resisting effects of liquid surface tension, static pressure and the drag on the bubble due to the relative motion between the bubble and liquid. The pressure balance over the bubble yields:

$$p_b = p_0 + \rho_l g(h - s) + \Delta p_\sigma + p_\mu + \frac{\rho_l h \ddot{V}}{A} + \rho_l[a\ddot{a} + 1.5(\dot{a})^2] \quad (1)$$

where, a is the bubble radius, V is the bubble volume $(4/3\pi a^3)$, atmospheric pressure, p_0, hydrostatic head, $\rho_l g(h - s)$, pressure due to surface tension, $\Delta p_\sigma = 2\sigma/a$, pressure due to viscous drag on bubble $\rho_\mu = 0.5 C_D \rho_l (ds/dt)^2$, pressure due to inertia of liquid caused by liquid translation, $\rho_l h \ddot{V}/A$, and pressure due to inertia of liquid surrounding the bubble, $\rho_l[a\ddot{a} + 1.5(\dot{a})^2]$

3.1.2. Force balance on the bubble

Force balance for a spherical rising bubble considering force due to added mass and neglecting Basset history force [1,6] yields Eq. (2). The last term in the force balance equation due to added mass of liquid surrounding the gas bubble. It is considered that the liquid mass corresponding to 1/2 of bubble volume move upward with the gas bubble [16] in the solution:

$$F_b - F_d - F_g = \frac{d}{dt}\left[\left(\rho_b + \frac{\rho_l}{2}\right) V \left(\frac{ds}{dt}\right)\right] \quad (2)$$

where F_b is the force due to buoyancy, F_d the drag force on the bubble, and F_g is the force due to gravity:

$$\frac{d}{dt}\left[\left(\rho_b + \frac{\rho_l}{2}\right) V \left(\frac{ds}{dt}\right)\right] = V(\rho_l - \rho_b)g - C_D \left(\frac{\pi a^2}{2}\right) \rho_l \left(\frac{ds}{dt}\right)^2 \quad (3)$$

Initial few pictures of the bubble rise are discarded to neglect the effect of the nozzle. Initial rise velocity is estimated from the change of position of bubble centroid in two successive frames.

The drag coefficient (C_D) depends on the bubble Reynolds number (Re), where the Re is defined as: $Re = 2a(ds/dt)\rho_l/\mu_l$, and where the drag coefficient for a bubble is [16]:

$$C_D = \frac{16}{Re}\left[1 + \left\{\frac{8}{Re} + \frac{1}{2}\left(1 + \frac{3.315}{Re^{0.5}}\right)\right\}^{-1}\right] \quad (4)$$

In the study the bubble Reynolds number was between 126 and 178.

3.2. Mass transfer from the bubble

3.2.1. Absorption mechanism and enhancement factor

The absorption of CO_2 from the gas bubble into NaOH solution takes place through the following two sequential steps [17]:

(1) Dissolution of gaseous CO_2 into aqueous NaOH solution at the gas/liquid interface.
(2) The diffusion of dissolved CO_2 in the liquid boundary layer accompanied by the chemical reaction with OH^- ions.

The overall rate of absorption is known to be controlled by the latter step of the simultaneous diffusion and chemical reaction in the liquid boundary layer.

The chemical reaction proceeds through the following sequential steps:

$$CO_2 + OH^- \rightarrow HCO_3^- \quad (5)$$

$$HCO_3^- + OH^- \rightarrow CO_3^{2-} + H_2O \quad (6)$$

Thus, the overall reaction can be written as

$$CO_2 + 2OH^- \rightarrow CO_3^{2-} + H_2O \quad (7)$$

It is a second order reaction between CO_2 and OH^-, and the stoichiometric factor z (number of OH^- ions reacting with one molecule of CO_2) is 2.

The equations for simultaneous diffusion with chemical reaction have been solved numerically by Brian et al. [18] and the results have been greatly condensed by him by introducing enhancement factor and some dimensionless terms:

$$\text{the enhancement factor, } E = \frac{\sqrt{M'(E_i - E/E_i - 1)}}{\tanh\sqrt{M'(E_i - E/E_i - 1)}} \quad (8)$$

where

$$M' = \frac{\pi}{4} k_r C_{B0} t \quad (9)$$

$$E_i = \sqrt{\frac{D_A}{D_B}} + \frac{C_{B0}}{zC_{A0}}\sqrt{\frac{D_B}{D_A}} \quad (10)$$

D_A and D_B are the diffusivities of dissolved CO_2 and NaOH, respectively. k_r is the kinetic constant for the reaction [19,20].

The enhancement factor signifies the factor by which the reaction increases the amount absorbed in a given time as compared to absorption without reaction.

3.2.2. Mass balance equation

Now the rate of mass transfer from the bubble can be expressed in terms of enhancement factor (E) as [21]:

$$\frac{dn_b}{dt} = -Ek_{LA}(4\pi a^2)C_{A0} \quad (11)$$

Mass transfer coefficient (k_{LA}) from Higbie's penetration theory:

$$k_{LA} = 2\sqrt{\frac{D_A(ds/dt)}{2\pi a}} \quad (12)$$

Analytical expression for enhancement factor (E) for second order reaction is according to Eq. (8).

According to Henry's law, the concentration of dissolved CO_2 in equilibrium with bubble pressure (p_b) is given by

$$C_{A0} = \frac{p_b}{H} \quad (13)$$

where Henry's constant H is determined by the method of Krevelen and Hoftizer [20]. Diffusivity of NaOH at finite dilution is determined using the equation of Gordon and Nernst [22].

Eq. (14) expresses the number of moles and pressure relationship:

$$p_b = \frac{n_b RT}{V} \quad (14)$$

Bubble density calculation is performed using the following equation:

$$\rho_b = \frac{n_b M_w}{V} \quad (15)$$

3.3. Contaminant accumulation stagnant cap model

3.3.1. Effect on mass transfer

The stagnant cap model of the bubble contamination proposed by Griffith [5] is used according to which the bubble contamination proceeds in four steps:

(1) Diffusion of contaminant from the bulk to the interface (mass transfer coefficient, k_s).
(2) Instantaneous adsorption of contaminant at the interface.
(3) Convection of contaminant by adjacent liquid towards the rear of the bubble.
(4) Accumulation of the contaminant molecules in a stagnant cap (area per mole, a_s), without desorption to the liquid.

If the surface convection is fast compared to both bulk diffusion and both the adsorption and desorption, the adsorbed contaminant is collected in a stagnant-cap region leaving the frontal region virtually uncontaminated (Fig. 3) and thus freely

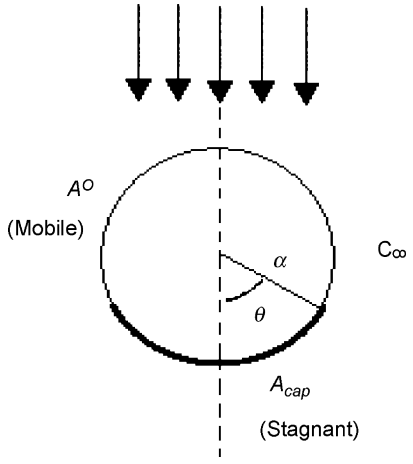

Fig. 3. Stagnant cap model.

mobile [9]. It is assumed that diffusion controls the contaminant transport from the bulk as if it were insoluble [6,23]. Stagnant cap size is a function of the bulk concentration of the contaminant and if the bubble is small enough, the cap may cover the entire surface [24]. It is assumed that the mass transfer from the bubble to the liquid phase occurs only from the mobile phase.

The rate of diffusion of contaminant from the bulk to the surface can be described by the rate equation as [9]:

$$\frac{dn_s}{dt} = k_s(A_b - A_{cap})C_\infty \tag{16}$$

If a_s is the area occupied by a mole of contaminant ($A_{cap} = n_s a_s$) and assuming that the mass transfer coefficient (k_s) obeys Higbie's relationship with some characteristic length assuming to be the bubble diameter ($d = 2a$) then:

$$k_s = k'(2a)^{-1/2}$$

where k' is a constant for a given gas diffusivity and given gas–liquid slip velocity. Lumping k', molar mass a_s and bulk concentration C_∞ into a single parameter k which may be assumed constant for a given bulk concentration:

$$k = k' a_s C_\infty \tag{17}$$

Therefore, the resulting equation for the growth of the contaminant surface with time is

$$\frac{dA_{cap}}{dt} = k(2a)^{-1/2}(A_b - A_{cap}) \tag{18}$$

Therefore, the bubble dissolution given by Eq. (11) changes to

$$\frac{dn_b}{dt} = -Ek_{LA}(4\pi a^2 - A_{cap})C_{A0} \tag{19}$$

3.3.2. Effect on drag coefficient

A simple relationship between drag force and the stagnant cap angle developed by Sadhal and Johnson [6] is used. This relationship is converted to the following expression of drag coefficient of the partially contaminated bubble in terms of the other drag coefficients:

$$C_D(\theta) = \frac{C_{D,rigid} - C_{D,mobile}}{2\pi} \times \left(2\theta + \sin(\theta) - \sin(2\theta) - \frac{1}{3}\sin(\theta)\right) + C_{D,mobile} \tag{20}$$

where $C_{D,rigid}$ and $C_{D,mobile}$ are the drag coefficients for bubbles with a rigid and mobile surface, respectively.

Improved values of $C_{D,mobile}$ is calculated using Eq. (4) and the drag coefficient ($C_{D,rigid}$) for a rigid particle is calculated following Clift et al. [1]:

$$C_{D,rigid} = \frac{24}{Re}(1 + 0.1935Re^{0.6305}) \tag{21}$$

Eq. (18) is solved to obtain the A_{cap}, the area occupied by the contaminant assuming an initial A_{cap}. The parameter k is obtained by fitting the model output to the experimental data of bubble radius, rise and velocity.

3.4. Initial conditions

Eqs. (1), (2) and (19) for the bubble growth, motion and mass transfer respectively are solved simultaneously with the initial conditions for p_b is derived from Eq. (1) by assuming $\ddot{a}$ to be small and neglecting the same at initial stage:

$$p_{b0} = p_0 + \rho_l g(h - s) + \frac{2\sigma}{a} + p_\mu + \left[\frac{8\pi\rho_l h a}{A} + \frac{3}{2}\rho_l\right]\dot{a}^2 \tag{22}$$

$$s_0 = 0 \tag{23}$$

for a known initial bubble radius a_0 with a known value of $(ds/dt)_0$ (from experimental data). MATLAB software was used for programming using the ODE45 integration routine.

4. Results and discussions

4.1. Parameter estimation

The parameter k in the stagnant cap model was treated as a best-fit parameter and obtained by fitting the model output with the experimental data for each concentration of NaOH for different bubble radius. It was estimated to be 0.0065, 0.008 and 0.0095 $m^{1/2}/s$ for 4%, 6% and 10% NaOH solutions, respectively. The increase in the value of k with NaOH concentration is probably due to higher amount of impurities in more concentrated solution.

4.2. Effect of initial concentration of NaOH solution

From the several experiments, data for three bubbles of almost same (maximum 0.62% deviation) initial observed radius (0.496 mm) were chosen. Actual bubble radii were 0.4952, 0.4991 and 0.4949 mm, respectively. The bubbles were rising in 4%, 6% and 10% NaOH solutions in the three experiments. The initial velocities of the bubbles were determined in each experiment from two initial frames of photographs. Initial pressure was estimated using Eq. (22). The initial liquid head on the bubble was considered to be same for all the bubbles.

4.2.1. Bubble size

Fig. 4 shows the change in the bubble radius with time from experiments and model. It is observed from the figure that the slope of the curve decreases with the initial concentration. This is because the dissolution rate with chemical reaction increases with the initial concentration of NaOH solution and hence the bubble radius reduces fast in 10% solution. It is also observed that the slope of the curve for a given initial concentration decreases after a certain time; this is because of the reduction of the interfacial area of bubble for the mass transfer due the added effect of the contaminants.

Fig. 5 compares the experimental and model fitted bubble radius. The dashed lines represent the maximum % absolute error of 11.5%. The mean % absolute error for the model is 6.89%. It is observed that for the model results are in good

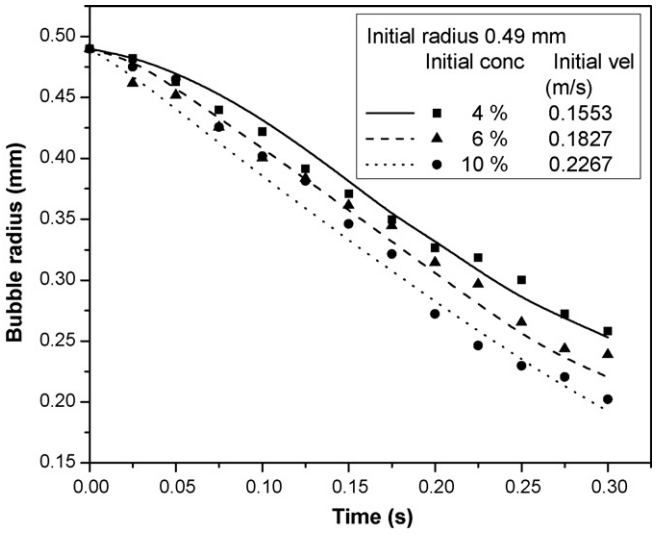

Fig. 4. Bubble radius with time—experimental and model fitted results.

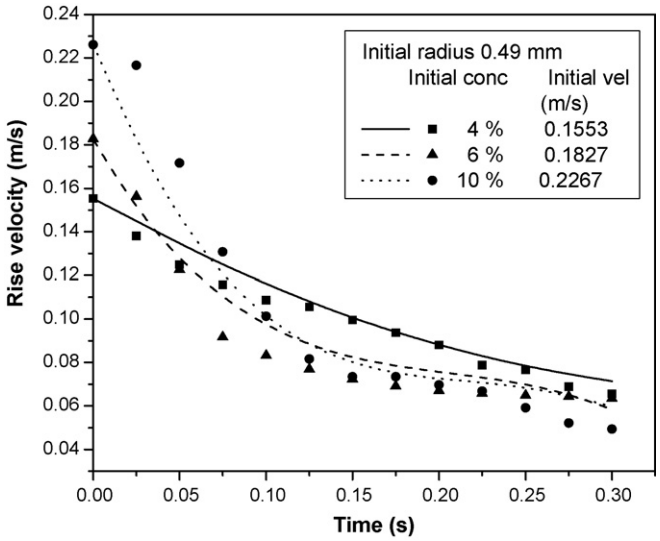

Fig. 6. Bubble rise velocity with time—experimental and model fitted results.

agreement with the experimental results in the range about 0.35–0.49 mm. The fit is poorer in the lower range of the bubble radius. This may be attributed to the higher inaccuracy in the measurement of the bubble radius at lower values.

4.2.2. Bubble rise velocity

Fig. 6 shows the change in bubble rise velocity during experiments and the same predicted from the model. Since the radius of the bubble and therefore the buoyancy on it decreases with time the bubble velocity decreased with time. It is also observed that the rate of decrease in the velocity is reduced after a certain time, this is because of the increase in drag and reduction of the mass transfer area and *lowered shrinking rate* of the bubble due to contaminant accumulation.

Fig. 7 compares the experimental and model fitted bubble rise velocity for experiments conducted with 4%, 6% and 10% NaOH solutions. The maximum % absolute error is about 24% and the mean % absolute error is about 8%. It is observed that the model best fits the experimental values at higher velocities, i.e. from around 0.09 m/s. The fit is poorer in the lower velocity range. The error in the lower range of the velocity (below 0.06 m/s) may be due to the error in the measurement of smaller size bubbles. It is also seen that the model has a tendency to over predict at higher velocities. This is possible as at higher velocity the bubbles are larger and larger size bubbles tend to flatten out and rise slowly compared to the spherical bubbles as assumed in the model.

4.2.3. Bubble rise

In general larger bubbles rise faster. It is observed from Fig. 8 that the bubble rise is high in a 4% solution as the mass transfer rate and the effect of contaminants are low in the low concentration solution. Rise of the bubble in 10% solution is comparable with that in the 4% solution, which is due to the effect of its higher initial velocity. It is also observed that the bubble rises faster initially and the rise is hindered after a certain time, which

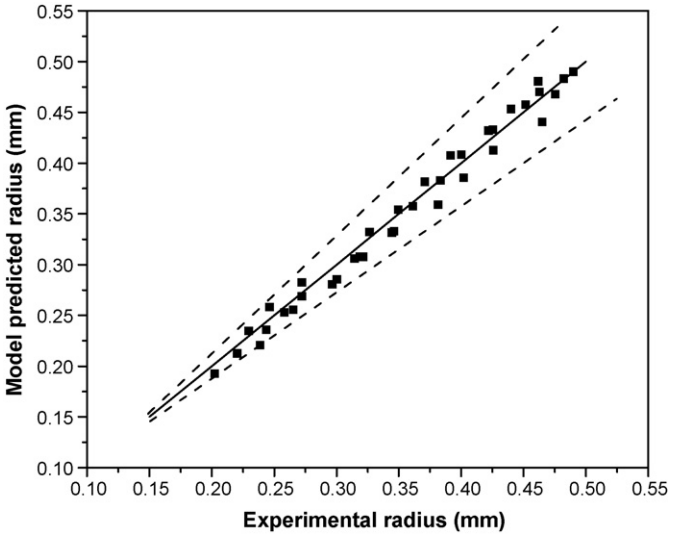

Fig. 5. Experimental and model fitted bubble radius.

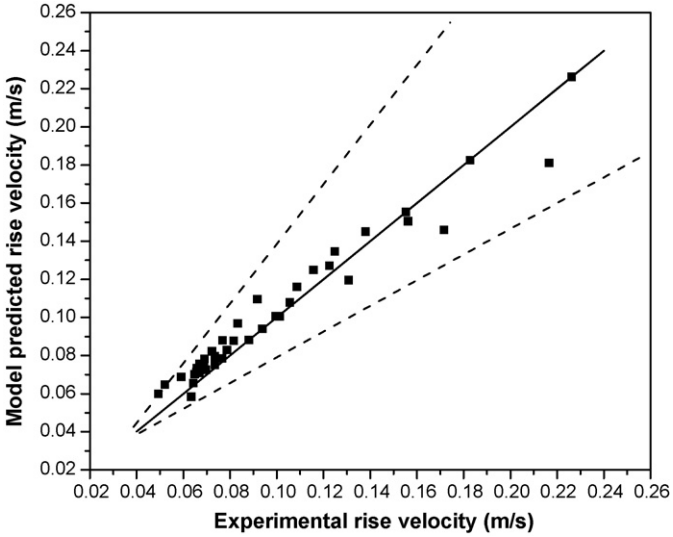

Fig. 7. Experimental and model fitted bubble rise velocity.

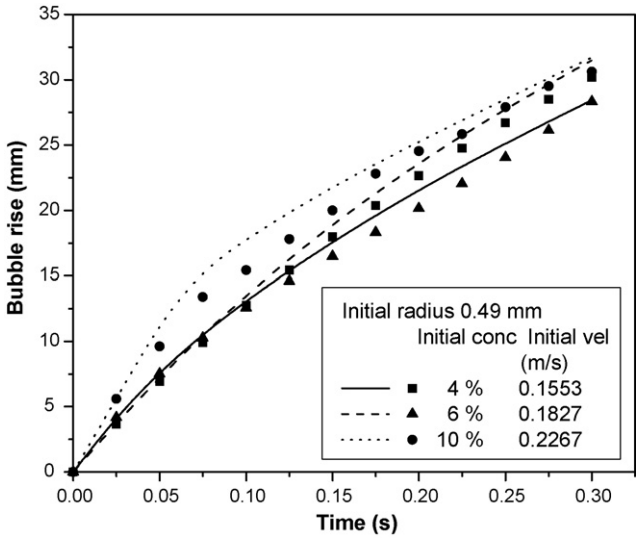

Fig. 8. Bubble rise with time—experimental and model fitted results.

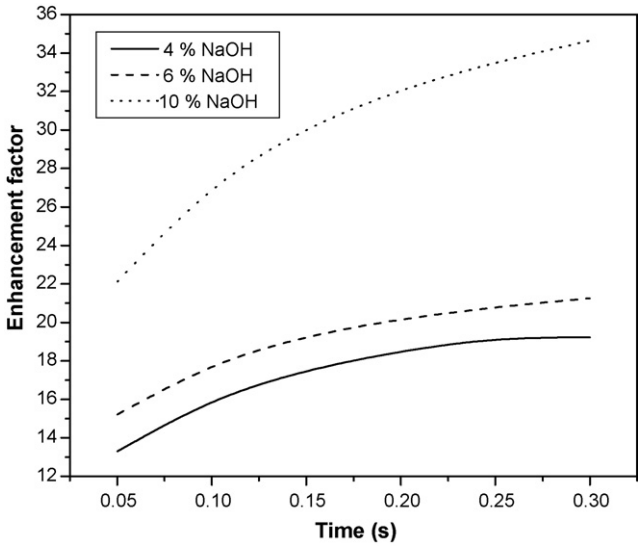

Fig. 10. Enhancement factor change with time predicted by the model.

is due to the effect of the accumulated contaminants and reduction in size due to reaction.

Fig. 9 compares the experimental and model fitted bubble rise for experiments conducted with 4%, 6% and 10% NaOH solutions. It is observed that the model fits the experimental rise with a maximum % absolute error of 15.3% and mean % absolute error of about 7.3%.

4.2.4. Enhancement factor

Fig. 10 shows the enhancement factors predicted by the model (Eq. (8)) for bubbles of initial radius 0.49 mm in 4%, 6% and 10% NaOH solution. It shows the amount by which the mass transfer is enhanced by the chemical reaction in different concentrations of NaOH. It is observed that the enhancement is high in solutions of higher concentration. This is because of high mass transfer with a chemical reaction of CO_2 in solutions of higher NaOH concentration.

4.2.5. Cap angle

The growth of cap angle with time in different concentrations of NaOH solutions predicted by the model (Eq. (18)) is shown in Fig. 11. It is seen that the cap angle gradually increases with the time; this is because of the continued accumulation of the contaminant on the surface of the bubble. It is observed that the cap angle in 10% solution is high, which is probably because of a larger amount of contaminant present in a higher concentration solution.

4.2.6. Drag coefficient

Fig. 12 shows the increase in the drag coefficient with time predicted by the model (Eq. (20)) in different concentrations of NaOH solution. It is observed that the drag coefficient on the bubble increases with the concentration of NaOH solution; this is because of the high viscosities and contaminants present in the 10% and 6% solutions. With the contaminants accumulated on

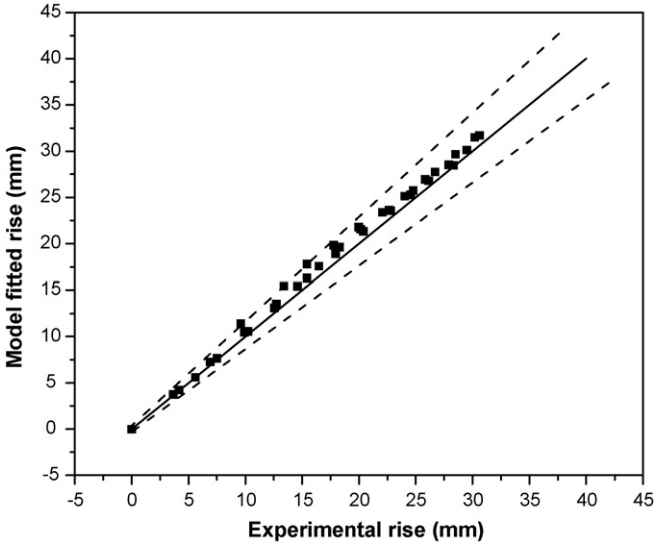

Fig. 9. Experimental and model fitted bubble rise.

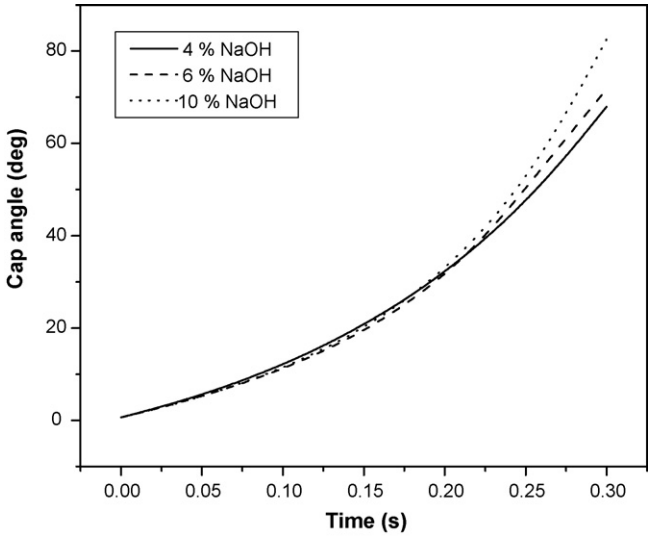

Fig. 11. Cap angle change with time predicted by the model.

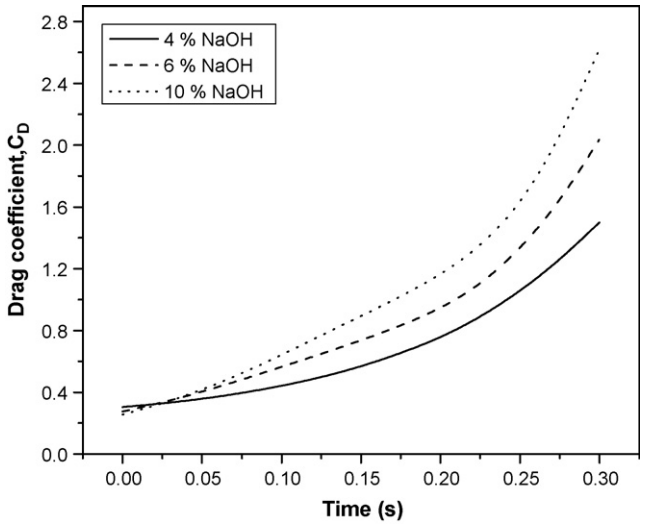

Fig. 12. Drag coefficient change with time predicted by the model.

the surface, the bubble tends to behave as a rigid sphere and the drag on the bubble changes from the mobile interface to that of a rigid surface. Therefore, it is observed that the increase in drag coefficient of a bubble in single concentration is low initially and then increases after a certain time

Fig. 13 shows the drag coefficient change with cap angle predicted by the model for different concentrations. It can be seen that the drag coefficient on the bubble increases with the cap angle since the drag and the cap angle increase with amount of the contaminant accumulated. The initial rise velocity order is in the order of increasing concentration of NaOH during experiments. Velocity, rise and cap angle affects C_D. Therefore, though the C_D is higher for higher NaOH concentration for same cap angle as observed, the same should not be taken as a general trend.

4.3. Effect of different initial bubble radius

A set of experimental results with initial bubble radii of 0.49, 0.58, and 0.63 mm in 4% NaOH solution were chosen for evaluating effect of initial bubble size. The initial velocities of the bubbles were 0.1553, 0.1843 and 0.1511 m/s, respectively.

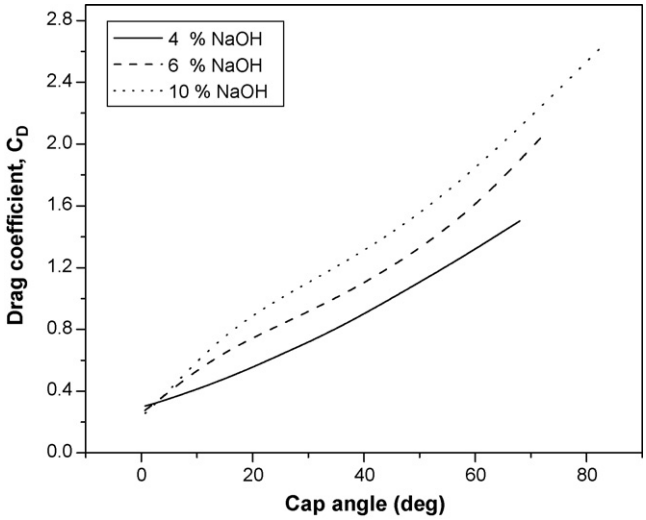

Fig. 13. Drag coefficient change with cap angle predicted by the model.

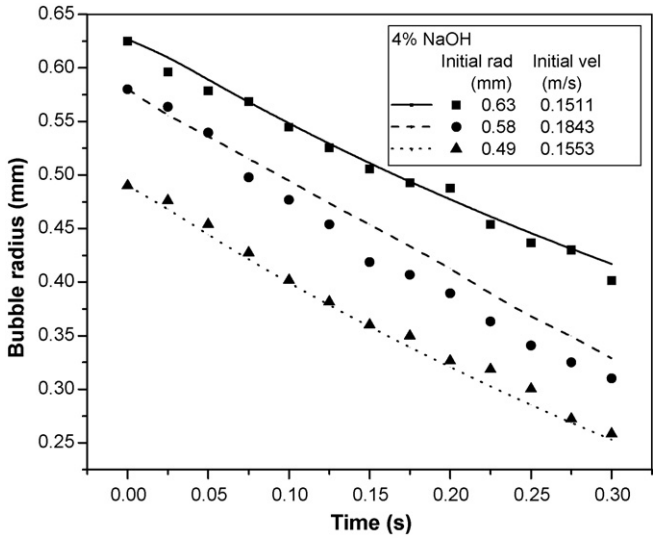

Fig. 14. Bubble radius with time—experimental and model fitted results.

4.3.1. Bubble size

Fig. 14 shows the change in the bubble radius with time from the experiments and that predicted from the model. The reduction rate of the bubble size is at almost same for 0.49, 0.63 mm, but the reduction rate of bubble size for the 0.58 mm initial radius is slightly higher. This is probably because the bubble with initial size 0.58 mm had a higher initial velocity (0.1843 m/s) compared to the others (0.1553 and 0.1511 m/s). A bubble with a high initial velocity travels a longer distance for a given time and hence has a higher dissolution. The reduction in the rate of the bubble radius decrease towards the end is because of contaminants accumulated on the surface of the bubble, i.e. stagnant cap effect.

4.3.2. Bubble rise velocity

Fig. 15 shows velocity transient of the bubbles of three different radii in 4% NaOH solution. From the above figure it can

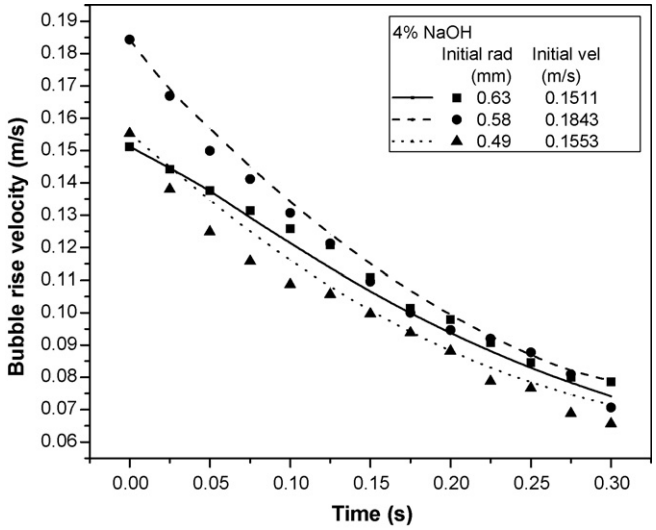

Fig. 15. Bubble rise velocity with time—experimental and model fitted results.

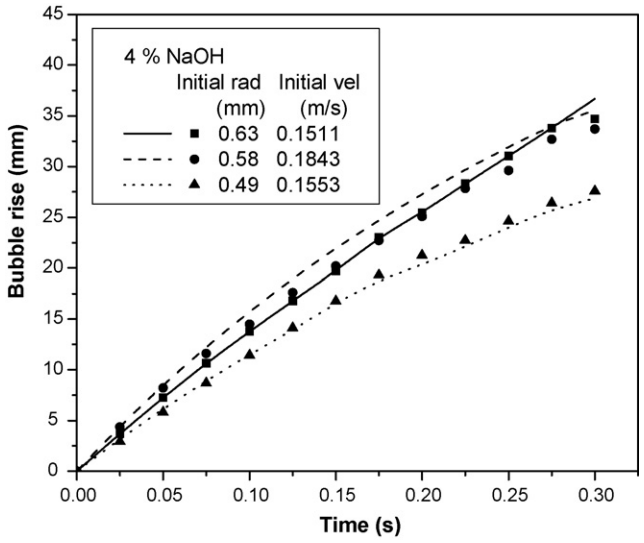

Fig. 16. Bubble rise with time—experimental and model fitted results.

be observed that the bubble with initial radius 0.49 and 0.63 mm having nearly the same initial velocity show decrease in velocity with the same rate. The bubble with higher radius, i.e. 0.63 mm has a higher velocity; this is because of its higher buoyancy when compared to the lower size bubble. The bubble rise velocity of 0.58 mm bubble at a given time is higher than the 0.63 mm bubble due to its high initial velocity.

4.3.3. Bubble rise

Fig. 16 shows the rise of bubbles with different radii in 4% NaOH solution. In the figure we observe that the bubbles with nearly same initial velocity but with lower initial radius rise at a slower rate. Lower buoyancy and higher drag coefficient on a smaller bubble explains this. The rise of a 0.58 mm bubble is comparable with that of the 0.63 mm bubble; this anomaly is probably due to its higher initial velocity. It is also observed that the rate of rise of the bubble reduces after a certain time, i.e. the slope of the curve decreases after a certain time, which is due to the additional drag from the accumulation of the contaminants.

4.3.4. Enhancement factor

Fig. 17 shows the amount by which the mass transfer is increased with reaction with time obtained from the model for bubbles of different radii in 4% NaOH. It is seen that the enhancement because of reaction is nearly the same in the bubbles with different radii. The enhancement because of the reaction depends mainly on the interface concentration of the gas and the initial concentration of NaOH solution, since the concentration of NaOH solution is constant here, and the change in the interface concentration of CO_2 for the bubbles of different radii is not high; the enhancement factor is nearly same for bubbles of different radii in a given concentration of NaOH solution.

4.3.5. Drag coefficient

Fig. 18 shows the variation of drag force predicted by the model for bubbles with three different radii. The bubbles with radii 0.63 and 0.49 mm have nearly same initial velocity. It is observed that the bubble with radius 0.49 mm has higher drag coefficient because of its lower Reynolds number compared to the larger bubble. The bubble with radius 0.58 mm initially has a high drag coefficient than that of 0.63 mm radius bubble due to its high initial velocity.

4.3.6. Cap angle

Fig. 19 shows the stagnant cap angle change with time for bubbles of radii 0.49, 0.58, 0.63 mm in 4% NaOH solution, predicted by the model. It is observed that the cap angle gradually increases with time; this is due to accumulation of the contaminants on the surface of the bubble. The cap angle in a smaller bubble is higher.

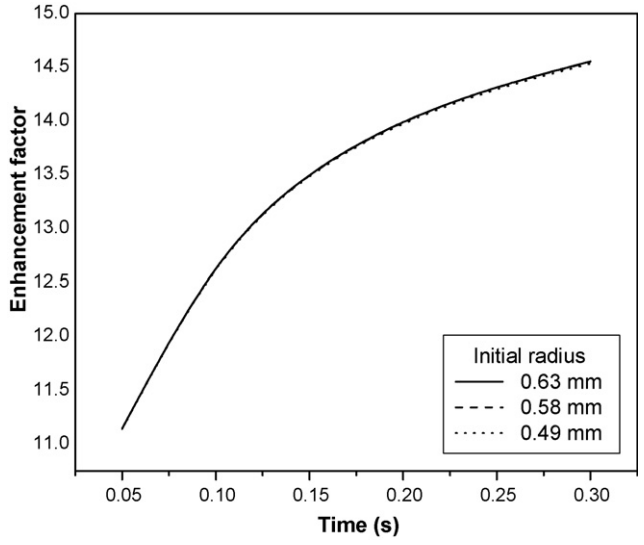

Fig. 17. Enhancement factor change with time predicted by the model.

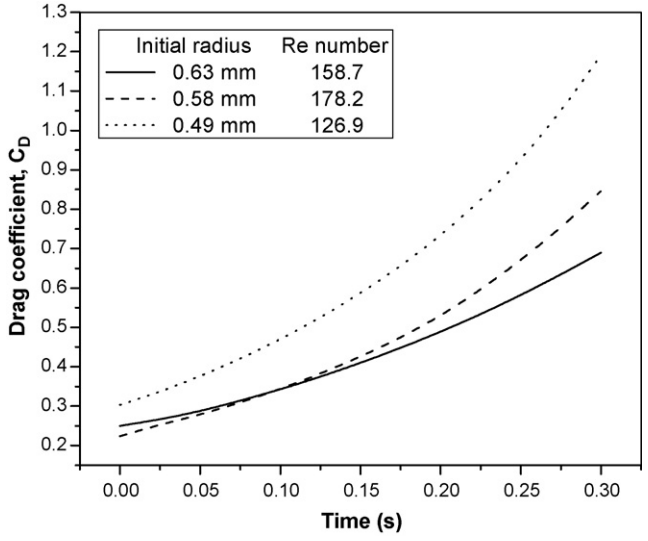

Fig. 18. Drag coefficient change with time predicted by the model.

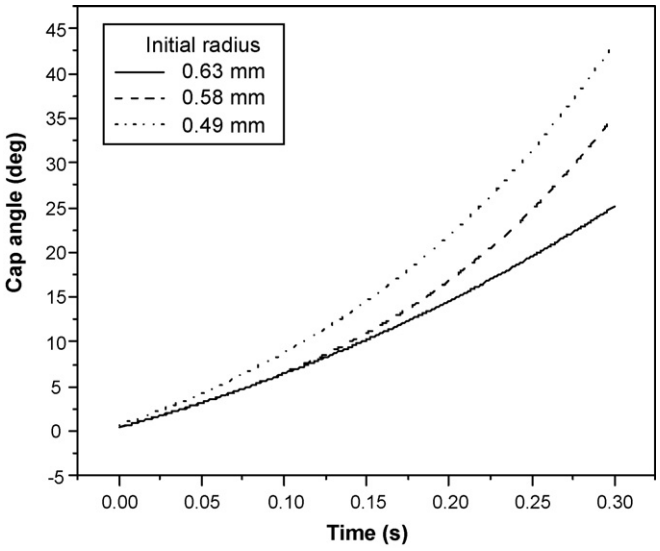

Fig. 19. Stagnant cap angle change with time predicted by the model.

5. Conclusion

The reactive bubble system of CO_2–NaOH system was studied for different concentrations of the NaOH (4%, 6% and 10%) solution and bubble sizes (0.45–0.65 mm). A simple dynamic model of the bubble based on pressure balance, force balance and mass transfer considerations has been developed. The model assumes sphericity of bubble, considers added mass of liquid, drag and surface tension effects on bubble pressure. It also includes the growth of stagnant cap on the bubble surface due to accumulation of contaminants. Predictions from this simple model are in good agreement with experimental results.

With the increase in the NaOH concentration it was found that bubble size reduces faster and these bubbles rise with lower velocity. Therefore, the bubble rise in same time is lower in high concentration solutions. Initial velocity of bubble significantly affects the bubble rise. Shrinking rate of the bubble after a certain time reduces due to the accumulation of contaminants on bubble surface.

When bubbles rise in NaOH solutions, rise and the velocity of initially larger bubble were found to be higher. Diameters of bigger and smaller bubbles diminish at nearly same rate. Enhancement factor is independent of bubble initial size. The drag coefficient and the cap angle was observed to be higher in small bubbles and increased with time. Due to the accumulation of the surfactants the drag coefficients increase.

References

[1] R. Clift, J.R. Grace, M.E. Weber, Bubbles, drops and particles, Academic Press, New York, 1978.
[2] G.E. Kinard, F.S. Manning, W.P. Manning, A new correlation for mass transfer from single spheres, Br. Chem. Eng. 8 (1963) 326–327.
[3] E. Ruckenstein, On mass transfer in the continuous phase from spherical bubbles or drops, Chem. Eng. Sci. 19 (1964) 131–214.
[4] H. Tsuge, S.I. Hamamoto, S.I. Hibino, Wall effect on the behavior of single bubbles rising in highly viscous liquids, J. Chem. Eng. Jpn. 17 (1984) 619–623.
[5] R.M. Griffith, The effect of surfactants on the terminal velocity of drops and bubbles, Chem. Eng. Sci. 17 (1962) 1057–1070.
[6] S.S. Sadhal, R.E. Johnson, Stokes flow past bubbles and drops partially coated with thin films. Part 1. Stagnant cap of surfactant film-exact solution, J. Fluid Mech. 126 (1983) 237–250.
[7] A. Tzounakos, D.G. Karamanev, A. Margaritis, M.A. Bergougnou, Effect of the surfactant concentration on the rise of gas bubbles in power-law non-Newtonian liquids, Ind. Eng. Chem. Res. 43 (2004) 5790–5795.
[8] G. Vizquez, M.A. Cancela, R. Varela, E. Alvarez, J.M. Navaza, Influence of surfactants on absorption of CO_2 in a stirred tank with and without bubbling, Chem. Eng. J. 67 (1997) 131–137.
[9] J.M.T. Vasconcelos, S.P. Orvalho, S.S. Alves, Gas–liquid mass transfer to single bubbles: effect of surface contamination, AIChE J. 48 (2002) 1145–1154.
[10] S.S. Alves, S.C.P. Orvalho, J.M.T. Vasconcelos, Effect of bubble contamination on rise velocity and mass transfer, Chem. Eng. Sci. 60 (2005) 1–9.
[11] F. Takemura, A. Yabe, Gas dissolution process of spherical rising gas bubble, Chem. Eng. Sci. 53 (1999) 2691–2699.
[12] F. Takemura, Y. Matsumoto, Dissolution of spherical carbon dioxide bubbles in strong alkaline solutions, Chem. Eng. Sci. 55 (18) (2000) 3907–3917.
[13] A. Brankovic, I.G. Curie, W.W. Martin, Laser-Doppler measurements of bubble dynamics, Phys. Fluids 27 (1984) 348–355.
[14] R.D. La Nauze, I.J. Harris, On a model for the formation of gas bubbles at a single submerged orifice under constant pressure conditions, Chem. Eng. Sci. 27 (1972) 2102–2105.
[15] S. Ray, S.P. Sengupta, Irreversibility analysis of a sieve tray in a distillation column, Int. J. Heat Mass Transfer 39 (1996) 1532–1542.
[16] R. Mei, J.F. Klausner, C.J. Lawrence, A note on the history force on a spherical bubble at finite Reynolds number, Phys. Fluids 6 (1) (1994) 418–420.
[17] Y. Fukunaka, Y. Jiang, T. Yamamoto, Z. Asaki, Y. Kondo, Nonuniformity of NaOH concentration and effective bubble diameter in CO_2 injection into aqueous NaOH solution, Metall. Transact. B 20B (1989) 5–12.
[18] P.L.T. Brian, J.F. Hurley, E.H. Hasseltine, Penetration theory for gas absorption accompanied by a second order chemical reaction, AIChE J. 7 (1961) 226–231.
[19] P.V. Danckwerts, A.M. Kennedy, The kinetics of carbon dioxide into neutral and alkaline solutions, Chem. Eng. Sci. 8 (1958) 201–215.
[20] P.V. Danckwerts, Gas–Liquid Reactions, McGraw-Hill Book Company, New York, 1970.
[21] R.B. Bird, W.E. Stewart, E.N. Lightfoot, Transport Phenomena, Wiley, New York, 1960.
[22] J. Perry, Chemical Engineers Hand Book, 4th ed., McGraw-Hill, New York, 1963.
[23] S.S. Ponoth, J.B. McLaughlin, Numerical simulation of mass transfer for bubbles in water, Chem. Eng. Sci. 55 (2000) 1237–1255.
[24] R.E. Davis, A. Acrivos, The influence of surfactants on creeping motion of bubbles, Chem. Eng. Sci. 21 (1966) 681–685.